Preprint Title Poly (1-Vinyl Imidazole) Polyplexes as Novel Therapeutic Gene Carriers for Lung Cancer Therapy

Authors Gayathri kandasamy, Elena N. Danilovtseva, Vadim annenkov and Uma maheswari Krishnan

Publication Date 07 Okt 2019

Article Type Full Research Paper

ORCID® iDs Elena N. Danilovtseva - https://orcid.org/0000-0002-7961-8158; Vadim annenkov - https://orcid.org/0000-0002-6616-154X; Uma maheswari Krishnan - https://orcid.org/0000-0001-6508-4485

Poly (1-Vinyl Imidazole) Polyplexes as Novel Therapeutic Gene Carriers for Lung Cancer Therapy

Gayathri Kandasamy[1], Elena N. Danilovtseva[2], Vadim V. Annenkov[2], Uma Maheswari Krishnan[1,*]

[1]Centre for Nanotechnology & Advanced Biomaterials (CeNTAB), School of Chemical and Biotechnology, SASTRA Deemed University, Thanjavur – 613401, Tamil Nadu, India

[2]Limnological Institute of the Siberian Branch of the Russian Academy of Sciences, 3, Ulan-Batorskaya St., P.O. Box 278, Irkutsk, 664033, Russia

[*]Corresponding author

Prof. Uma Maheswari Krishnan Ph. D.
Dean, School of Arts, Science & Humanities
Professor, School of Chemical & Biotechnology
Centre for Nanotechnology & Advanced Biomaterials (CeNTAB)
SASTRA Deemed University, Thanjavur – 613 401
Tamil Nadu,
India

Ph.: (+91) 4362 264101 Ext: 3677

Fax: (+91) 4362 264120

E-mail: umakrishnan@sastra.edu

Abstract

The present work explores the ability of poly (1-vinyl imidazole) to complex si-RNA against vascular endothelial growth factor (VEGF) and its in vitro efficiency in A549 lung cancer cells. The polyplex formed was found to exhibit 66% complexation efficiency. The complexation was confirmed by gel retardation assay, FTIR and thermal analysis. The blank PVI polymer was not toxic to cells. The polyplex was found to exhibit excellent internalization and escaped the endosome effectively. The polyplex was more effective than the free si-RNA in silencing VEGF in lung cancer cells. The silencing of VEGF was quantified using Western blot which was also reflected in depletion of HIF-1α levels in the cells treated with the polyplex. VEGF silencing by the polyplex was found to augment the cytotoxic effects of the chemotherapeutic agent 5-fluorouracil. Microarray analysis of the mRNA isolated from cells treated with free siRNA and polyplex reveal that the superior VEGF silencing by the polyplex altered the expression levels of several other genes that have been implicated in the proliferation and invasion of lung cancer cells. These results indicate that PVI complexed anti-VEGF can be an effective strategy to counter lung cancer.

Keywords

Poly (1-vinyl imidazole), gene silencing, anti-VEGF si-RNA, lung cancer

Introduction

Gene therapy is a promising strategy that can be employed for treatment of many hereditary disorders as well as diseases triggered by sporadic mutations including many forms of cancers. However, the therapeutic potential of gene therapy is yet to be realized completely due to the challenges associated with its stability, target-specificity and transfection. [1] Use of viral or non-viral vectors to deliver the therapeutic oligonucleotide to the target cell has been widely explored to overcome the inherent problems associated with administration of the naked oligonucleotide. [2] Majority of gene delivery studies have employed viral vectors due to their superior transfection capabilities. But the high frequency of mutations and packing limitations associated with viral vectors necessitate the search for safer alternates. [3] In this context, non-viral vectors have garnered interest in recent years as gene delivery vehicles. But the highly cationic nature of the carriers employed is associated with immunogenicity and toxicity. Further, the ability of these carriers to escape the acidic endosomes in the cells limit their transfection efficiency. [3] One of the widely explored non-viral polymeric carrier for gene delivery is poly (ethylene imine) that can effectively escape from the endosomes through the 'proton sponge' mechanism. [4] However, PEI systems are limited by their toxicity and hence there arises a need for a less toxic but effective gene carrier.

The imidazole ring is involved in many physiological processes and therefore imidazole containing systems have been investigated for a myriad of biological applications. [5] Poly (vinyl imidazole) is a water-soluble polymer that has been synthesized as poly(1-vinylimidazole) and poly (4-vinyl imidazole) [6] by different methods. The imidazole groups can be protonated in acidic pH thereby conferring cationic character to the polymer. The conformation of PVI chains were found to be altered on protonation that is dependent on the anions present in the system. [7] Several studies have explored the potential biomedical applications of PVI and its derivatives. Pullulan grafted poly (N-vinyl imidazole) was found complex the anionic citrate and tripolyphosphate effectively in acidic medium due to the imidazole. [8] The catalytic properties of poly(1-vinylimidazole) due to the proton-donating nature of the imidazole group have been demonstrated in few reports. [9] These films demonstrated excellent anti-microbial effect. [10] A copolymer of poly (acrylamide) and poly (vinylimidazole) was used as a hydrophilic matrix to disperse multi-walled carbon nanotubes and the glucose oxidase enzyme for glucose sensing applications. [11] A hydrogel of xanthan gum and poly (N-vinyl imidazole) was recently explored for protein encapsulation and delivery. The system exerted no toxic effects on cells and maintained the functionality of the protein. [12] Pyrrole-N-imidazole polyamide system was found to inhibit prostate cancer progression through interfering with the expression and function of the androgen receptor. [13] Chitosan-imidazole derivatives have been also explored for gene transfection in HEK293 cells. [14]

In recent years, poly (vinyl imidazole) (PVI)-based systems have emerged as a front-runner for gene delivery applications due to their polycationic nature, biocompatibility as well as ability to escape the endosome by activating the proton sponge mechanism. In an earlier report, histidylated poly (L-lysine) was found to exhibit high transfection efficiency enabled by the pH responsive endo-lysosomal escape (Jong-Eun Ihm P-4v). It was therefore expected that poly (vinyl imidazole)

side chains will show better transfection efficiency. Alkylated poly (1-vinyl imidazole) with different chain lengths has been investigated for DNA complexation and transfection efficiency in HepG2 liver cancer cells. The butylated PVI was found to be non-toxic and the most effective when compared to other alkyl derivatives towards DNA complexation.[15] Carboxymethyl poly (1-vinyl imidazole) has also been investigated for DNA complexation and were found to exert no toxicity to cells. [16] Poly (1-vinyl imidazole) chains modified with aminoethyl groups demonstrated excellent DNA binding ability in synergy with lactosylated poly (L-lysine). This system was found to exhibit excellent gene transfection ability specifically in hepatocytes through interactions with the asialoglycoprotein receptor expressed on the hepatocyte surface through the lactosylated poly (L-lysine). The endosomal escape was mediated through pH responsive protonation of the imidazole and amino moieties that disrupted the endosomal membrane. [16] Zinc-PVI systems have also been investigated for complexing DNA for gene delivery applications. [17]

Folic acid conjugated amine containing poly (1-vinyl imidazole) was found to effectively complex DNA and transfect cancer cells. [18] PVI linked with the dipeptide Cys-Trp was demonstrated to self-assemble to micelles that could also complex effectively with RNA. Very few studies have also attempted to investigate the DNA complexation efficiency of poly (4-vinyl imidazole) polymers that have demonstrated that it also possesses low cytotoxicity and good endosomal escape properties. [5]

It is evident from the scan of literature that only few proof-of-concept studies have been carried out to explore the potential of PVI as a cyto-compatible gene carrier. The present work aims to synthesize poly (1-vinyl imidazole) and explore for the first time its ability to deliver anti-VEGF si-RNA to curb the proliferation of lung cancer cells.

Materials and Methods

Materials

PVI was obtained by polymerization of a 30% ethanolic solution of 1-vinylimidazole in the presence of 2% (by monomer mass) of 2,2 -azobis(isobutyronitrile) in argon atmosphere at 60 ^{o}C by Prof. Annenkov's group and the polymer fraction with molecular weight 35,000 Da was used for the study. Detailed synthesis and characterization of the polymer was earlier reported by Prof Annenkov [19]. Lung cancer cell line A549 was procured from the National Centre for Cell Sciences (NCCS), Pune. HUVEC (human umbilical vein endothelial cells) was procured from ATCC, USA. Dulbecco's modified Eagle's medium (DMEM), Fetal bovine serum (FBS), Phosphate buffered saline (PBS) and Trypsin were purchased from Gibco, USA. EGM^{TM} – Endothelial Cell Growth Medium Bullet kit was procured from Lonza, USA. The VEGF si-RNA sequence (Sense 5' GGAGUACCCUGAUGAGAUC TT 3') (Antisense 5' GAUCUCAUCAGGGUACUCCTT3') and Cyanine-3 fluorescent tagged si-RNA (Sense: 5' CY3 GGAGUACCCUGAUGAGAUCTT 3') (Antisense: 5' CY3 GAUCUCAUCAGGGUACUCC TT 3') with λ_{ex} of 550 nm and λ_{em} of 570 nm were purchased from Eurofins Genomics, USA. Ribogreen reagent was purchased from

Invitrogen, USA. All other reagents of analytical grade were purchased from Merck, India. 5-FU (5-Fluorouracil) was procured from Sigma-Aldrich, USA. VEGF antibody (Santa Cruz Biotechnology Ltd., USA). β- actin and other antibodies (Cell Signaling Technology, USA) were used in the study. Microarray consumables were purchased from Cell Signaling Technology, USA. RNAse-free water was used for preparation of buffers and all solutions.

Methods

Preparation of the PVI-si-RNA polyplex

The stock solution of PVI ((poly) 1-vinyl imidazole)) was prepared using RNAse-free water at a concentration of 100 mg/mL. The pH was maintained at 7.0. The si-RNA stock solution was prepared at a concentration of 10 µM using RNAse-free water. For complexation, the aqueous solutions of PVI and si-RNA were mixed at different ratios (v/v). The resultant mixture was vortexed followed by incubation for 30 min at room temperature.

Characterization of the polyplex

Electron microscopy

A small drop of the polyplex sample was placed on a conducting carbon tape and air dried. The sample was then sputter coated with a thin film of gold using the sputter-coated. The sample was placed in the sample chamber and imaged at an accelerating voltage of 3 kV using a cold field emission scanning electron microscope (JSM6701F, JEOL, Japan). For transmission electron microscopy, 1 mL of the polyplex was deposited on 400 mesh copper grids (Canemco-Marivac, Canada) and air dried for 10 min. The excess sample was removed by blotting using a filter paper. The grids were washed using RNAse-free water and dried overnight. The samples were stained with 1% phosphotungstic acid solution (Merck, Germany) and imaged using high resolution field emission transmission electron microscopy (JEM2100F, JEOL, Japan).

Differential scanning calorimetry

The melting points of the blank PVI nanoparticles and the PVI-si-RNA polyplex was recorded using differential scanning calorimetry (DSC, Polyma 214, Netzsch, Germany) between the temperature range 0 and 300 ^{o}C in a nitrogen atmosphere at a scan rate of 5 ^{o}C / min. The samples were placed in an aluminium pan with lid that also served as the reference.

Fourier Transform Infrared Spectroscopy (FTIR)

The FTIR spectra for the free si-RNA, blank polymer nanoparticles and the polyplex were recorded between 4000 and 400 cm^{-1} averaging 10 scans /run in the attenuated total reflection mode (ATR) using Fourier transform infrared spectrometer (Spectrum 100, Perkin Elmer, USA).

Dynamic Light Scattering (DLS) and Zeta potential measurements

The hydrodynamic size of the PVI-si-RNA polyplexes was measured on a Zetasizer Nano ZS (Malvern instruments, UK). Samples at different volume ratios containing a final si-RNA concentration of 100 nM were used for the measurements. The measurements were made using quartz microcell of 1 mL capacity and 3 mm path length. Clear disposable cells were employed for measurement of zeta potential. All measurements were performed for each sample in triplicates 20 min after sample preparation at 25 ^{o}C.

Electrophoresis

The polyplexes with a tracking dye (bromophenol blue, 2 µL), were loaded on a 1% agarose gel. The electrophoresis was carried in Tris-boric acid buffer (TBE) buffer at 80 V for 45 min. The gel was visualized after staining with ethidium bromide in a UV transilluminator using a Gel Documentation system (Fusion SoloX, Vilber Lourmat, France) and imaged.

Heparin displacement assay

Polyplexes were prepared in the volume ratio of 4:1 with final si-RNA concentration of 100 nM and incubated with heparin (low molecular weight fraction, Sigma-Aldrich, USA) solutions of different concentrations for 30 min and expressed as heparin:si-RNA (v/v) ratio. The samples were electrophoresed on a 1% agarose gel containing 0.5 µg/mL ethidium bromide at 80 V for 20 min. The bands were visualized using the gel documentation system.

***In vitro* studies**

Cell viability

The effect of the blank polymer and polyplex was determined using MTS (3-(4, 5-dimethylthiazol-2-yl)-5-(3-carboxymethoxyphenyl)-2-(4-sulfophenyl)-2H-tetrazolium) assay (Cell Titer 96 Aqueous one solution, Promega, USA). Four thousand A549 cells per well were cultured in a 96-well plate at 37 ^{o}C in 5 % CO_2. Once the cells became confluent, the medium was removed, washed with PBS (phosphate buffered saline, pH 7.4) the non-adherent cells were removed. The polyplexes containing si-RNA was dissolved in 100 µL of serum-free media to the cells such that the concentration of si-RNA in each well was 100 nM. The medium was replaced with fresh medium after 4 h followed by incubation for specified time points (24 h or 48 h). MTS reagent (20 µL) along with 200 µL of serum-free media were added to each sample well and incubated at

37 ºC for 2 h. The reaction was terminated by 10% sodium dodecyl sulfate (SDS) solution. The absorbance was read at 490 nm using a multimode reader (Epoch i2, Biotek, USA). For assessing the effect of VEGF silencing on the cytotoxicity of 5-FU, the cells were initially treated with the polyplex or free si-RNA at a si-RNA concentration of 100 nM for 4 h. The medium was then replaced with fresh medium to which 400 μM of 5-FU was added and incubated for 48 h. The cell viability was then assessed using the MTS reagent as previously described.

Internalization studies

Internalization of the polyplex in A549 cells was investigated using Cy3 fluorophore-tagged si-RNA. A549 cells at a seeding density of 10^5 cells/well were cultured on a cover slip in a 6-well plate. When the cells reached confluency, the medium was removed and the non-adherent cells were removed by washing with PBS. The polyplexes containing fluorescent si-RNA were added to 100 μL of serum-free media such that the final concentration of si-RNA in the system was 100 nM. At pre-determined time points, the cells were stained with Hoechst 33258 and imaged using laser scanning confocal microscopy (FV1000, Olympus, Tokyo, Japan).

Anti-angiogenesis assay

HUVECs were seeded at a density of 2 x10^5/well in a 6-well plate. After 24 h, the medium was replaced with serum-free medium and left overnight. The change in morphology with formation of tubular network was monitored using an inverted microscope (Eclipse Ti, Nikon, Japan). Then, the cells were treated with the samples (free si-RNA or polyplex) containing a final concentration of 100 nM of si-RNA and incubated for specified time points. The cells were imaged using an inverted microscope to observe the effect of the treatment on the tubular network.

Migration assay

To evaluate the gene silencing effect of the polyplex, cell migration assay was performed using A549 cells. The cells were cultured in a 6-well plate with a seeding density of 10^5 cells/well. After the cells attained confluency, the non-adherent cells were removed after removal of the medium and washed with PBS. The polyplex containing 100 nM anti-VEGF si-RNA was added to 100 μL of serum-free media. After 4 h, the medium was replaced with fresh medium. A straight scratch was made in the well using a pipette tip to remove the cells in the scratch zone. Cell migration was observed after 48 h and the images were captured using light microscope. The migration rate was compared with untreated cells as well as cells treated with equivalent quantity of blank PVI nanoparticles and 100 nM of free si-RNA. The relative migration ability of the cells in each case was calculated as follows:

$$Relative\ migration\ rate\ (\%) = \frac{(Width\ of\ the\ cell - free\ zone\ at\ time\ 0 - Width\ of\ the\ cell - free\ zone\ at\ time\ 48\ h\ )}{Width\ of\ the\ cell - free\ zone\ at\ time\ 0} \times 100$$

Gene expression analysis

The VEGF gene silencing was determined using RT-PCR (AG22331, Eppendorf, Germany). About $3^{\times}10^5$ A549 cells were incubated with PVI, free si-RNA and the polyplex. The si-RNA concentration was maintained at 100 nM in all the *in vitro* experiments. 48 h of post-incubation, the cells were harvested for RNA isolation. RNA was isolated using Trizol (Invitrogen, USA) and quantified using Nanodrop (Thermo Instruments, USA). The quantified RNA was then converted to cDNA using iScript cDNA synthesis kit (BioRad, USA). The cDNA was amplified using VEGF specific primer and quantified using SYBR green (BioRad, USA). The relative gene expression was calculated using ΔΔCt method. β-actin was used as the house-keeping gene. The sequences of the primers used in the study are given in Table 1.

Table 1: Primers used for gene expression studies

Primers	Forward	Reverse
VEGF	5´-TGCCCACTGAGGAGTCCAAC-3'	5´-TGGTTCCCGAAACGCTGAG-3 '
β-actin	5‘- CTCTTCCAGCCTTCCTTCCT-3'	5´ -AGCACTGTGTTGGCGTACAG-3'

Western blot analysis

Total protein was isolated from the A549 cells using cell lysis buffer (1x RIPA buffer, PMSF, 1% protease and protease inhibitors cocktail) (Cell Signaling Technology, USA) was quantified using Lowry’s method. An aliquot of the cell lysate containing 50 µg protein was loaded in 12% sodium dodecyl sulfate-polyacrylamide gel. The membrane was blocked for 1 h with blocking buffer (5% skimmed milk in Tris-buffered saline containing 0.1% Tween-20) followed by overnight incubation primary antibody (VEGF antibody, dilution 1:500, Santa Cruz Biotechnology, USA) at 4ºC. The blots were then washed and incubated 1 h with appropriate anti-mouse horseradish peroxidase-conjugated secondary antibodies (dilution 1:5000, Cell Signaling Technology, USA) at room temperature. The protein spots were visualized using tetramethyl benzidine/hydrogen peroxide (TMB/H_2O_2, Bio-Rad, USA) reagent. Membranes were stripped, reblocked, and re-incubated with the primary antibody against the housekeeping protein β-actin (Cell Signaling Technology, USA). The images were acquired using gel documentation system (Fusion SoloX, Vilber Lourmat, France). The Bio-1D software was used for analysis of the images and the intensity of the bands was calculated. The background was normalized, and the intensity obtained for β-actin band was used to normalize the band intensity of the corresponding VEGF protein band.

Microarray analysis

For performing microarray analysis, the quality of the total isolated RNA was checked using gel electrophoresis. The microarray experiment was performed using oligonucleotide microarrays (Genechip - Primeview human, Affymetrix, USA) that can detect expression of 49,372 genes. Typically, 500 ng of RNA was converted to double-stranded cDNA. The biotin-labelled complementary RNA (cRNA) was amplified using *in vitro* transcription (IVT) of the second-stranded cDNA template using T7 RNA polymerase. 12 µg of the purified cRNA was fragmented using divalent cations at elevated temperature. The labeled fragmented sample was loaded into Primeview® Genechip and the chip was hybridized overnight at 45^{o}C, 60 rpm in the Genechip Hybridization Oven 645. The chip was washed and stained in the Fluidic Station FS450. The chip was then scanned using Genechip Scanner 3000 7G. The data analysis to identify differentially regulated genes in the cells treated with polyplex when compared with cells treated with free si-RNA was performed using Transcriptome Analysis Console v3.0 (Affymetrix, USA.) Fold values > 2.0 were considered as up-regulated and fold values < -2.0 were considered down-regulated.

Statistical Analysis

One way ANOVA was performed to assess the statistical significance of the data obtained for the cell viability, gene expression, protein expression and migration assay. The level of significance was found using Kruskal-Wallis statistical test or Bonferroni comparison test. $p < 0.05$ was considered significant.

Results and Discussion

The complexation of si-RNA with PVI was determined at different polymer:si-RNA ratios and the results are presented in Figure 1A.

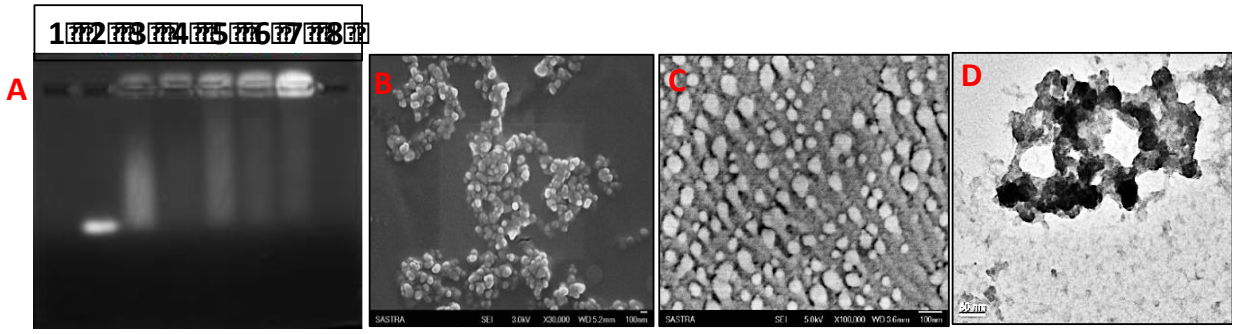

Figure 1: (A) Gel retardation assay for polyplexes formed with different ratios (v/v) of PVI:*si*-RNA. Lane 1: Blank, Lane 2: Free si-RNA, Lane 3: Polyplex formed with 1:1 ratio of PVI:si-RNA, Lane 4: Polyplex formed with 2:1 ratio of PVI:si-RNA. Lane 5: Polyplex formed with 3:1 ratio of PVI:si-RNA, Lane 6: Polyplex formed with 4:1 ratio of PVI:si-RNA, Lane 7: Polyplex formed with 8:1 ratio of PVI:si-RNA, Lane 8: Blank; (B) Scanning electron micrograph of blank polymer nanoparticles (C): Scanning electron micrograph of

polyplex formed with polymer:si-RNA ratio (v/v) of 4:1: (D): Transmission electron micrograph of polyplex formed with polymer:si-RNA ratio (v/v) of 4:1

The free si-RNA content progressively decreases with increasing polymer concentration while the complexed form exhibits a corresponding increase in intensity. The maximum intensity was observed at 4:1 ratio of polymer to si-RNA. A slight amount of uncomplexed RNA is observed even at the polymer: si-RNA ratio of 4:1 which corresponds to a N/P ratio of 250. These results were confirmed by the ribogreen assay where it was observed that about 66% of si-RNA was complexed at the 4:1 ratio of PVI:si-RNA. The imidazole nitrogen are protonated at acidic pH [20] while the complexation was carried out at physiological pH of 7.4 where considerably lesser number of imidazole nitrogen are protonated. This leads to high N/P ratios required for complexation. Though the polyplex ratio of 8:1 also exhibits superior complexation, 4:1 ratio was preferred as very high concentrations of the polymer may impede the release of the si-RNA.

The quantification of the Figures 1B to 1D show the scanning electron micrographs and transmission electron micrograph of the polyplex formed at the PVI:si-RNA ratio of 4:1. Formation of spherical nanoparticles in the size range of 80 to 120 nm is clearly discernible from the electron micrographs. The hydrodynamic diameter of the blank PVI nanoparticles measured using dynamic light scattering was found to be about 237 ± 34.6 nm. The zeta potential measured for the blank PVI nanoparticles in HEPES buffer of pH 7.4 was found to be 16.2 ± 2.76 mV while it reduced to 12.3 ± 0.92 mV after complexation with si-RNA. The shift in the zeta potential values indicate the formation of the PVi-si-RNA polyplex that has resulted in the alteration in the surface charges.

The complexation of si-RNA with PVI was investigated by FTIR and DSC (Figure 2). The FTIR of PVI shows vibration bands at 2950 cm^{-1} due to the the C-H stretch and at 1645 cm^{-1} and 1506 cm^{-1} and 1411 cm^{-1} due to C-N stretching vibrations due to the imidazole rings. The N-H in-plane bending vibrations are observed at 1235 cm^{-1}. The polyplex also shows stretching vibrations at 1635 cm^{-1}, 1501 cm^{-1} and 1427 cm^{-1} due to C-N vibrations and at 1235 cm^{-1} due to the N-H in plane bending vibrations. The band appearing at 573 cm^{-1} in the FTIR spectra of the polyplex and blank si-RNA may be attributed to the phosphate groups of the oligonucleotide clearly confirming the complexation.

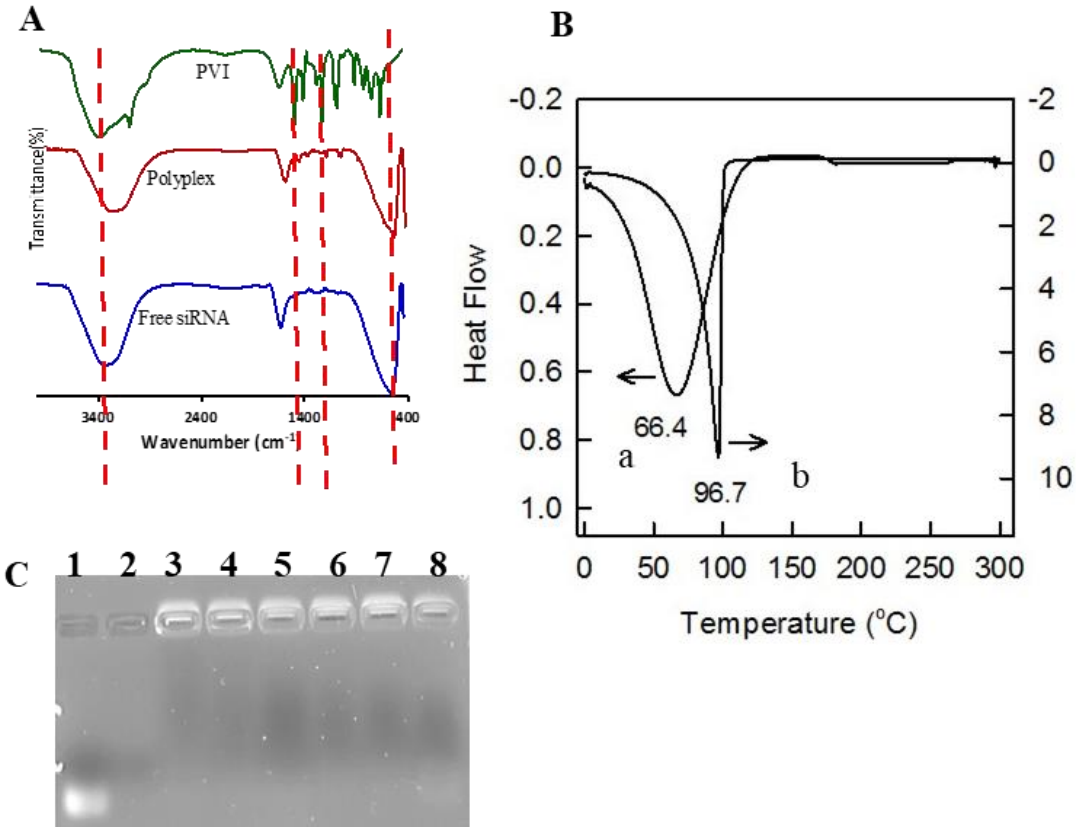

Figure 2: (A): FTIR spectra of free si-RNA, PVI and the polyplex; (B): Heat flow profile for pristine PVI (a) and polyplex (b) in nitrogen atmosphere, (C): Heparin displacement assay for the polyplex at different concentrations of the heparin. Lane 1: Free si-RNA, Lane 2: 60 ng/mL of heparin only, Lane 3: heparin:polyplex ratio (w/w) of 0.5, Lane 4: heparin:polyplex ratio (w/w) of 1, Lane 5: heparin:polyplex ratio (w/w) of 1.5, Lane 6: heparin:polyplex ratio (w/w) of 2, Lane 7: heparin:polyplex ratio (w/w) of 2.5, Lane 8: heparin:polyplex ratio (w/w) of 3

The differential thermal calorimetric profile (Figure 2B) reveals that the melting point for the pristine polymer is about 65 ^{o}C which exhibits a positive shift to 98 ^{o}C upon complexation with si-RNA. This can be attributed to the electrostatic interactions between the anionic phosphate moieties in the si-RNA with the cationic imidazole groups in the polymer resulting in an increase in the melting point for the polyplex.

The stability of the polyplex in serum is a major factor that could influence its therapeutic efficacy. The serum proteins could dissociate the si-RNA-polymer complex thereby reducing the delivery efficiency. Heparin is a glycosaminoglycan that is associated with inhibition of the coagulation process by activating anti-thrombin. [21] The sulphate groups present in heparin compete with the

oligonucleotide sequences to associate with the polymer chains and based on the relative strength of the electrostatic interactions between the oligonucleotide and polymer, heparin may succeed in displacing the oligonucleotide from the polyplex. Our results show an absence of free si-RNA on successive addition of heparin to the polyplex. The stability of the polyplex is maintained even when the heparin:polyplex ratio (w/w) reaches 3. This indicates good serum stability of the polyplex.

***In vitro* studies**

The internalization of the polyplex in A549 cells were determined at different time points and the results are presented in Figure 3.

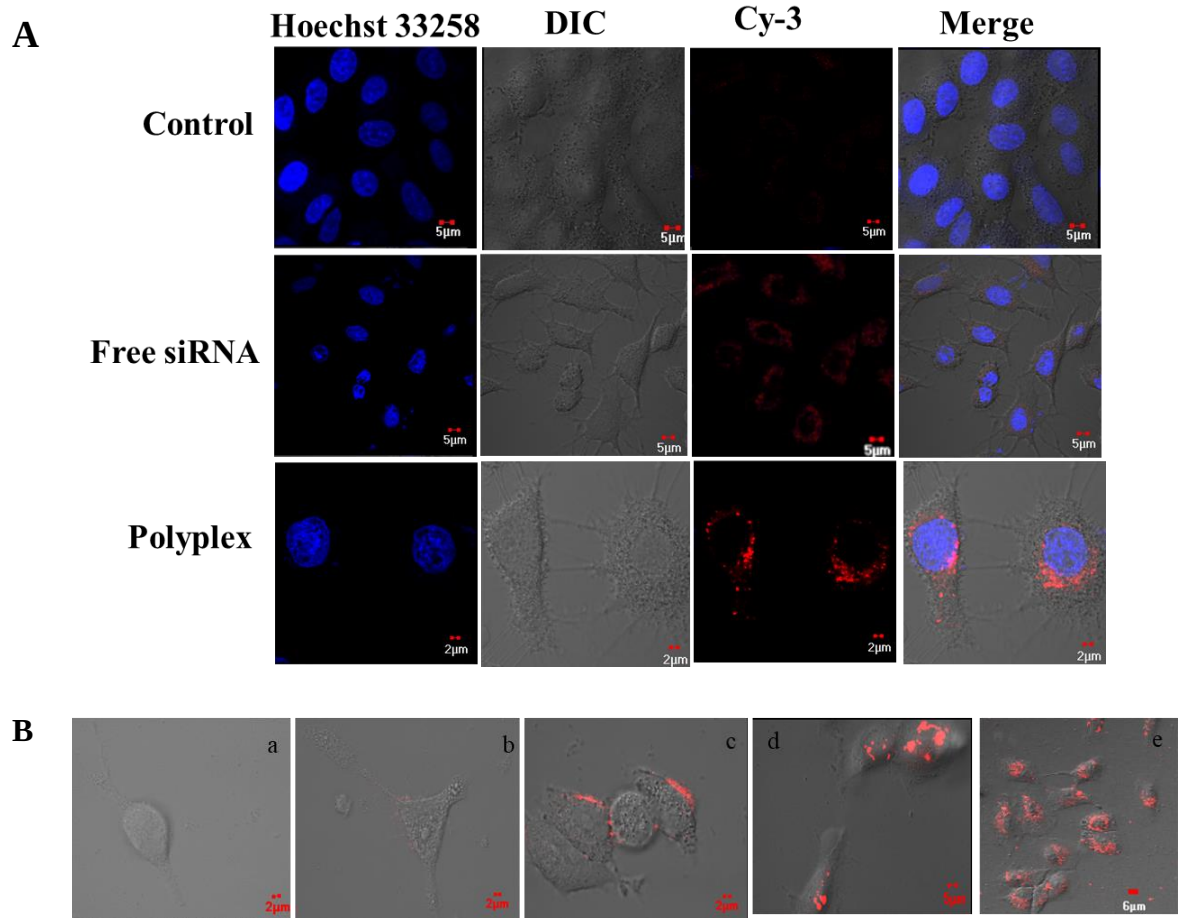

Figure 3: (A) Intracellular uptake of the polyplex were monitored using laser scanning confocal microscopy after 4 h of treatment with Cy3-labeled anti-VEGF si-RNA at final si-RNA concentration of 100 nM and complexation in the volume ratio of 4:1. Untreated cells were used as control. Nuclei were stained with Hoechst 33258 (blue). (B) Intracellular uptake of the polyplex at different time points. a: Control, b: 30 minutes,c:1 h,d: 4 h,e: 16 h

It is observed that the PVI polyplexes accumulate on the membrane surface after 15 minutes and start internalizing in to the cells after 30 min. Two hours post-administration, the polyplexes are found to be inside the cells and remain even after 16 hours (Figure 3B). The localization of the polyplexes was found to be the cytosol which is preferable for gene silencing as the RISC [22] is formed in the cytoplasm.

Most of the gene delivery systems become ineffective in delivering their cargo due to their inability to escape the endosome in cells. To investigate ability of the PVI polyplex to escape from endosomes, their co-localization with the endosomes was investigated and the results are presented in Figure 4.

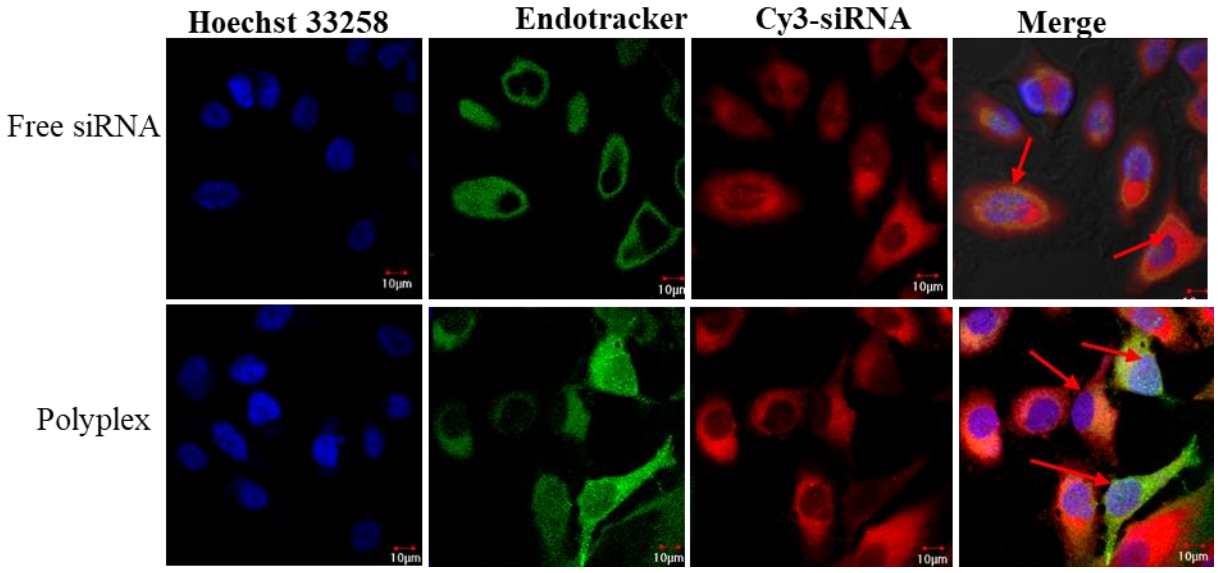

Figure 4: The endosomal escape of the polyplex after 4 h of incubation in A549 cells using endotracker (stains early endosomes green) and red fluorescence from Cy-3 labeled si-RNA observed by confocal laser scanning microscope. The co-localization of the Cy3-labeled si-RNA and endosome were observed as yellow fluorescence (red arrows).

The green fluorescence of the endosomes and red fluorescence of the fluorophore-tagged si-RNA are perfectly merged indicating that the free si-RNA is unable to escape from the endosomes. This is on expected lines as it has been established earlier that double stranded oligonucleotides tend to accumulate in the endosomal compartment and very few manage to reach the cytosol. [23] The polyplex treated cells reveal several zones of red fluorescence localized at regions distinct from the green fluorescence. This suggests that a fraction of the polyplex has escaped from the

endosomal compartment which is advantageous for gene delivery applications. The imidazole moieties in PVI can neutralize the acidic pH due to their basic nature which in turn can aid their endosomal escape through proton sponge mechanism, altering the membrane permeability or by-passing the endosomes. [24] However, the confocal images also reveal that a fraction of the polyplex identified by the red fluorescent zones also co-localize with the endosomes that fluorescence green. This suggests that a part of the polyplex remains in the endosome and may not be able to contribute to the silencing.

The effect of the polyplex on the viability of A549 lung cancer cells was investigated after 48 h and the results are shown in Figure 5. After 48 h, the cells treated with 100 nM of free si-RNA and blank polymer exhibited viabilities exceeding that of the untreated control cells while those cells treated with the polyplex exhibited a decreased viability.

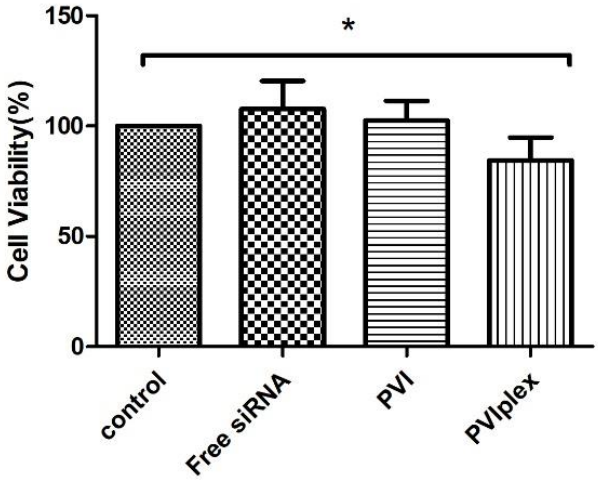

Figure 5: Cell viability of A549 cancer cells after treatment with carrier systems (blank as well as after complexation with anti-VEGF si-RNA). The A549 cells displayed lower viability after 48 h of treatment ($p < 0.05$ vs control), n = 5.

VEGF inhibition has been earlier reported to decrease the proliferation of cancer cells due to its ability to interfere with the MAPK and PI3K/Akt signaling pathways [25] which could be reflected in the viability values. The absence of any inhibition in the cell viability by the blank polymer indicates its cyto-compatibility while the lack of activity in the case of free si-RNA may be due to its inability to escape from the endosome. The complexation of the si-RNA with PVI results in better internalization as well as promotes endosomal escape thereby aiding its ability to form RISC (RNA-induced silencing complex) to cleave VEGF mRNA.

The morphology of the cells treated with the blank polymer and the polyplex are compared with the untreated control cells and the results are presented in Figure 6.

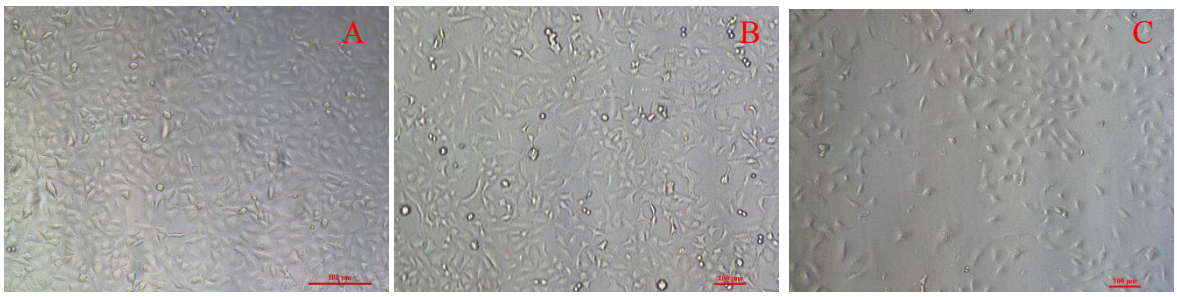

Figure 6: Morphology of A549 cells with and without treatment. A: Control, B: Blank polymer nanoparticles, C: Polyplex

Though significant changes in the morphology are not observed post-treatment with si-RNA complexes, subtle reduction in the tendency of the cells to interact with each other is discernible in the PVI-si-RNA complex treated cells where the cells appear to lose their contacts with each other. This may auger well for cancer therapy as the treatment may retard spheroid and stroma formation. VEGF signaling has been implicated in activation of the focal adhesion kinases and paxillin leading to cell morphology changes promoting migration. [26] Therefore, inhibition of VEGF leads to reduction in the formation of cell-cell junctions that are a primer for the cell migration. The treatment with blank polymer did not show any changes in the clustering of cancer cells indicating that the observed change is solely due to VEGF inhibition by the PVI polyplex.

The effect of VEGF si-RNA silencing on migration was investigated using cells treated with free si-RNA or polyplex for 48 h (Figure 7). It is observed that the gap created was filled slowly in cells treated with free si-RNA when compared with the control cells. This was even more delayed in cells treated with the polyplex and pristine PVI. It is likely that the polymer also exhibits a retarding effect that in combination with VEGF silencing interferes with the migration potential of the cancer cells.

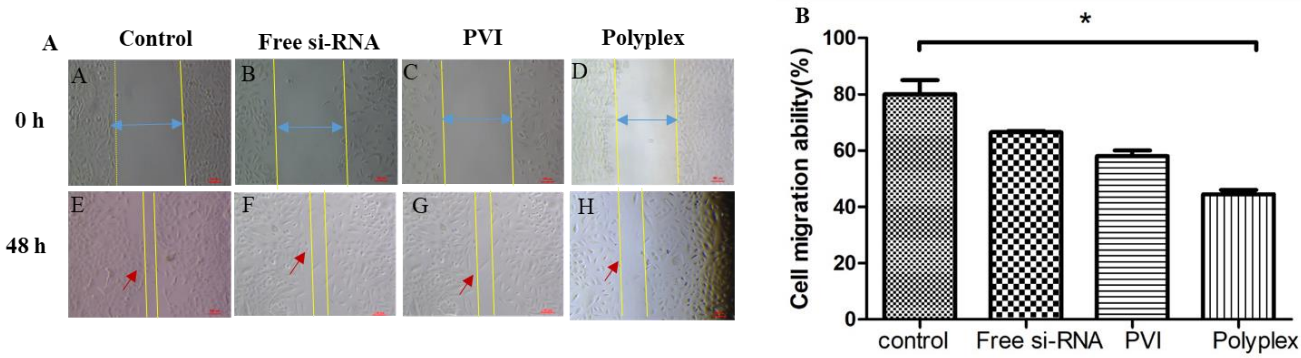

Figure 7: (A): Migration of A549 cells 48 h after treatment with free si-RNA, blank polymer nanoparticles and polyplex. VEGF silencing decreases the migration of A549 cells. Cells were exposed to the anti-VEGF si-RNA for 4 h. (B): Migration rate of the A549 cells 48 h after treatment with the samples, n = 3, p < 0.05 vs control

VEGF inhibition can also be used in combination with chemotherapeutic agents to enhance their therapeutic efficacy. The ability of the polyplex to alter the cell viability of A549 cells treated with 5-FU was investigated and the results are represented in Figure 8. The cells were first treated with the polyplex for 4 h followed which the medium was replaced, and different concentrations of 5-FU were added, and the viability was determined after 48 h. Imidazole and its derivatives have been earlier shown to inhibit migration of cancer cells and also their invasiveness. [27] Our results show that PVI also with its multiple imidazole groups can retard the migration of A549 cancer cells.

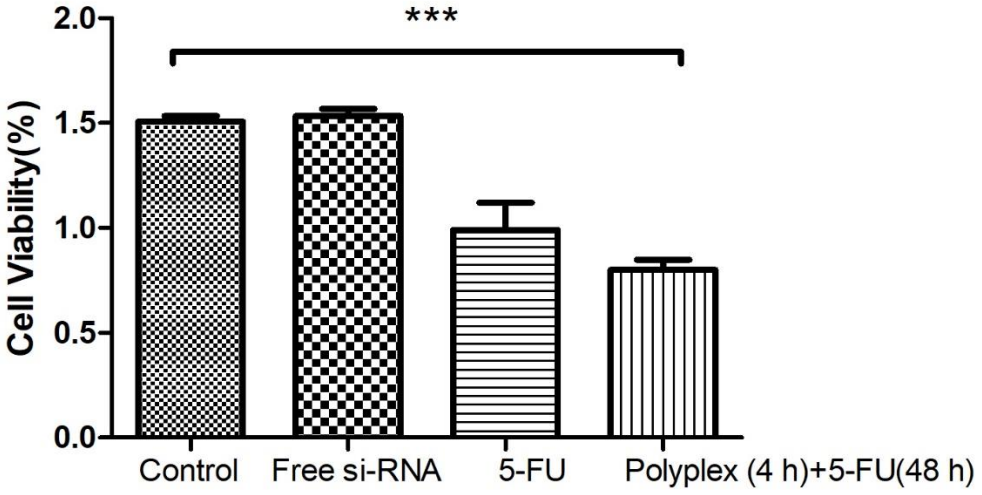

Figure 8: Viability of A549 cells after silencing VEGF using free si-RNA or the polyplex for 4 h followed by treatment with 5-FU for 48 h. A final concentration of 100 nM si-RNA and 400 µM of 5-FU were used in A549 cells and shown as mean ± SD (n=3). ***p<0.05 compared with control.

It is observed that the cell viability of A549 lung cancer cells decreased when pre-treated with polyplex for 4 h followed by treatment with 5-FU for 48 h. The free 5-FU exhibited a decrease in cell viability by 77% at 400 µM concentration while free si-RNA reduced the viability to 80% at 100 nM concentration. But in the presence of VEGF-loaded polyplex, the same concentration of 5-FU reduced the viability of A549 cells to 57% indicating that VEGF silencing sensitizes the cells to 5-FU. Similar observations have been recorded in hepatoma cells that were sensitized to doxorubicin following VEGF silencing. [28]

VEGF is a key factor that initiates angiogenesis and hence its silencing is expected to influence the formation of new blood vessels. Human umbilical vein endothelial cells (HUVECs) have been extensively used to monitor the effects of pro-angiogenic and anti-angiogenic factors. The HUVECs respond to serum starvation by enhancing the expression of hypoxia inducible factors (HIF-1α) that activate VEGF. This is manifested by distinct changes in the morphology of the HUVECs that become elongated and associate to form chains and tubular structures. Figure 9 shows the changes that occur in the morphology of HUVECs at 0, 24 h and 48 h in serum-free medium. The high magnification image of HUVECs after 48 h shows formation of elongated tubular assembles that are characteristic of neo-angiogenesis. Figure 9 shows the effect of PVI polyplex treatment on the morphology of HUVEC cells in serum-free medium. A distinct alteration in the morphology of the HUVECs is observed characterized by the absence of distinct elongation and tube formation in the cells clearly indicating the effect of VEGF inhibition.

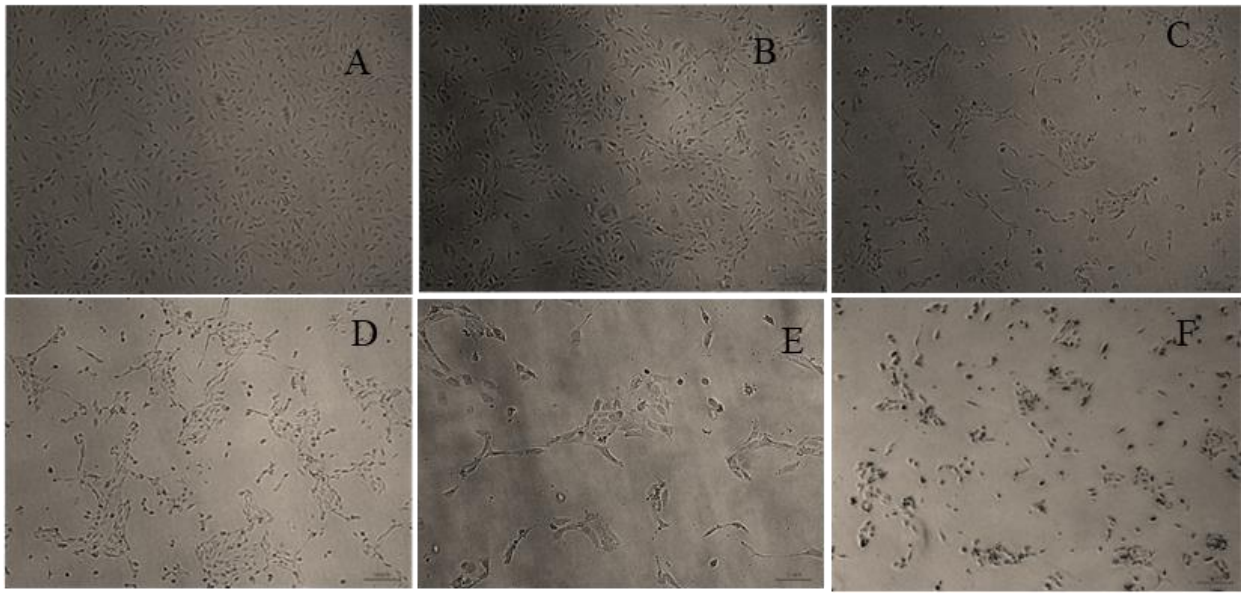

Figure 9: Morphology of HUVECs cultured in serum-free medium after (A): 0 h, (B): 24 h (C):48 h, (D): Control (E) & (F) 4 h after treatment with PVI-si-RNA complex

Earlier studies have identified that VEGF binds to $\alpha_9\beta_1$ integrin on the cell surface that mediates he formation and migration of endothelial cells through Src and focal adhesion kinase. [29,30] Therefore, silencing of VEGF by the polyplex was found to retard tube formation and extension of the endothelial cell processes in the present study.

Microarray analysis

Figure 10 shows the microarray data obtained for the genes deregulated by treatment with the polyplex in A549 cells after 48 h when compared with those treated with the free si-RNA and untreated cells. A fold change of 2 or above was considered for analysis.

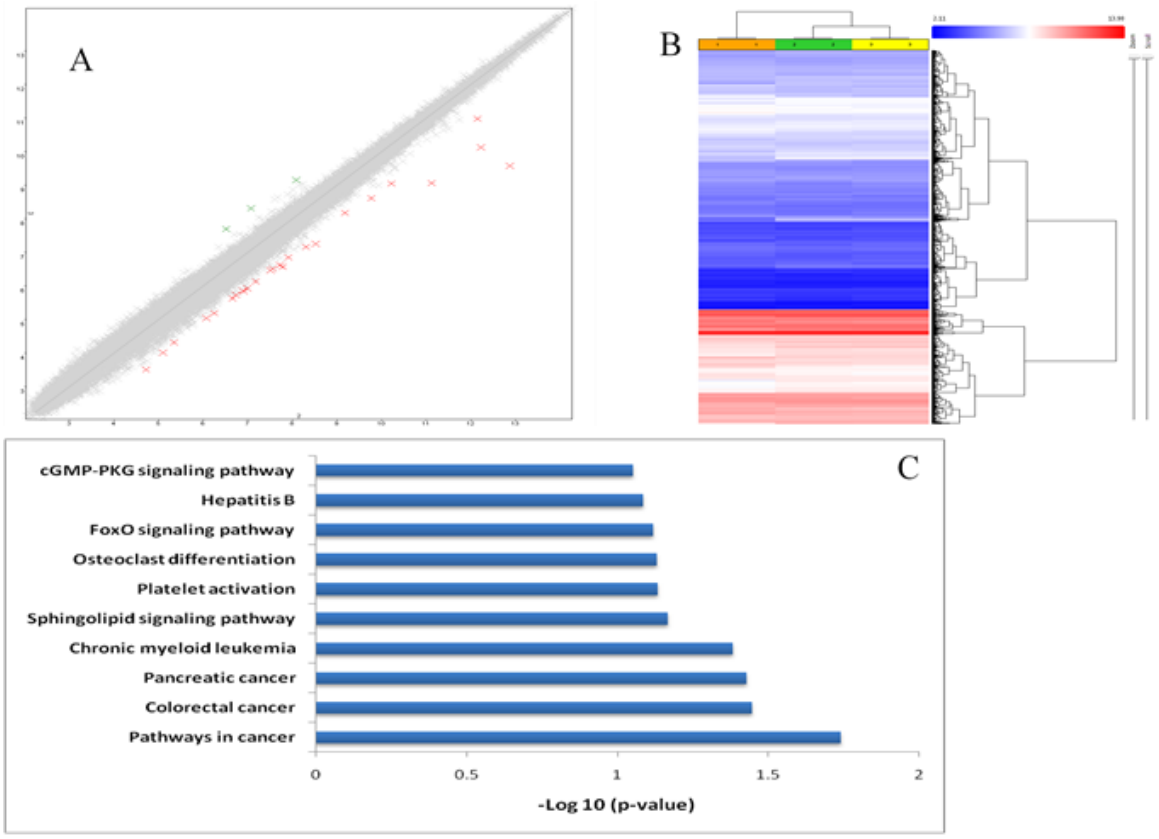

Figure 10: (A): Gene expression profile of the polyplex vs anti-VEGF si-RNA obtained from the microarray analysis, (B): Heat map obtained from the microarray analysis for control, free si-RNA and polyplex treated cells, (C) The KEGG pathway indicating the number of genes modulated by the polyplex treatment in A549 cells when compared with the free-si-RNA treatement.

Table 2 lists the gene targets that were found to be differentially altered by the polyplex treatment when compared to the cells treated with free-si-RNA.

Table 2: Genes that were differentially regulated by the polyplex when compared with the cells treated with free si-RNA

S.No	Fold change	Gene	Description
1	-2.08	GREM1	Gremlin 1, DAN family BMP antagonist
2	-2.09	GNA13	Guanine nucleotide binding protein (G protein), alpha 13
3	-2.01	PHF6	PHD finger protein 6
4	2.35	TFF1	Trefoil factor 1
5	-2.04	BROX	BRO1 domain and CAAX motif containing
6	2.09	ZNF440	Zinc finger protein 440
7	2.28	CEMIP	Cell migration inducing protein, hyaluronan binding
8	-2.06	AKT3	v-Akt murine thymoma viral oncogene homolog 3
9	-2.04	TGFBR1	Transforming growth factor, beta receptor 1
10	-2.32	TOR1AIP2	Torsin A interacting protein 2
11	-2.06	FAM169A	Family with sequence similarity 169, member A
12	-2.13	UBAP2	Ubiquitin associated protein 2
13	-2.08	LCLAT1	Lysocardiolipin acyltransferase 1
14	-2.14	CHP1	Calcineurin-like EF-hand protein 1
15	-2.06	RFC5	Replication factor C (activator 1) 5, 36.5kDa

VEGF has been implicated in a variety of signaling pathways in cancers that are now being revealed through gene and protein expression studies. In order to identify the effect of VEGF silencing on the various gene targets in A549 cells, a microarray analysis was performed and the relative change in expression levels of genes in cells treated with free si-RNA and the polyplex was compared to study the merits of using a polymeric carrier for delivery of anti-VEGF si-RNA. TFF1 was found to be up-regulated in the polyplex treated cells when compared to the free si-RNA group. The role of TFF1 in cancer remains controversial but many reports have demonstrated that TFF1 serves as a tumor suppressor gene that inhibits cancer cell proliferation and migration in epithelial cancers such as gastric, breast and pancreatic cancers. [31] Recent experimental evidence has revealed that TFF1 when complexed with TFIZ1 exhibits a tumor suppressor activity while it transforms in to a tumorigenic molecule when present in the uncomplexed state. [32] Among the genes that are down-regulated in the cells treated with the polyplex when compared to the cells treated with free si-RNA is PHF6 (PHD finger protein 6). This gene has been found to be differentially expressed in different types of cancer. It is now found that this gene is overexpressed in several epithelial cancers including breast and colorectal and serves as an oncogene. [12] Its down-regulation may therefore be a positive indicator for lung cancer therapy. Silencing of PHF6 has been shown to inhibit migration of hepatocellular cancer cells. [33] Other gene targets that are down-regulated in the polyplex treated cells when compared with the free si-RNA treated cells are TGFBR1, the transforming growth factor beta receptor 1 and Akt3. [34] TGF-β is involved in the

proliferation of cancer by activating the phosphorylation of SMAD and subsequent nuclear translocation of transcription factors. [34] Interestingly, TGF-β has been implicated in angiogenesis through activation of VEGF. Therefore, the down-regulation of TGFBR1 gene is a consequence of the superior VEGF silencing properties exhibited by the polyplex. TGF-β has also been implicated in promoting cancer cell migration. [35] Our migration assay data shows that the polyplex retards migration which suggests that VEGF-mediated silencing by the polyplex and down-regulation of PHF3 and TGF-β could have contributed to this retardation in migration potential of the A549 cells. Akt [36] has three isoforms that have now been identified to possess different effects on the progression and invasiveness of lung cancer. [37] A recent report has demonstrated a direct relation between the expression levels of Akt3 and VEGF.[38] Therefore, the reduced Akt3 expression in cells treated with the polyplex is a direct consequence of its superior VEGF silencing ability. A related target that is suppressed in the polyplex treated cells is GREM1 gene that encodes for Gremlin1, a key protein in the TGF-β signaling pathway, which is overexpressed in many cancers, including lung cancer. [39] Gremlin1 is involved in the survival of the tumor cells and promotes the formation of the stromal barrier. [39] It has also been identified as an agonist of VEGF and its receptor VEGFR2. [39] Therefore, better VEGF silencing by the polyplex is manifested through GREM1 down-regulation in polyplex treated cells when compared to its free si-RNA counterparts. Down-regulation of CHP-1 (calcineurin b homologous protein 1) gene in cells treated with the polyplex when compared to the free si-RNA treated cells is also linked to the inhibition of angiogenesis. Indirect evidence from earlier reports have implicated that inhibition of CHP-1 is linked with the inhibition of HIF-1α, a key target in the angiogenesis pathway involving VEGF. The polyplex treated cells had decreased levels of GNA13, UBAP2, RFC5, LCLAT1 and BROX genes when compared with the cells exposed to free si-RNA. GNA13 [40] is a target that has been associated with the proliferation and metastasis of many types of cancers. [40] Recent evidence has shown that high levels of GNA13 expression mediates angiogenesis through elevation of VEGF levels. Our data reveals that the inhibition of VEGF can also suppress the GNA13 expression, which in turn could be beneficial for controlling the proliferation and invasion of lung cancer. LCLAT1 (lysocardiolipin acyltransferase1) has been implicated in the regulation of cardiolipin, a key membrane phospholipid. LCLAT1 has been associated with establishing endothelial lineages. [41] Independent studies have revealed elevated levels of LCLAT1 in colorectal and lung cancers that augments the unregulated proliferation and metastasis of the cancer cells. [41] Though direct involvement of LCLAT1 in modulating VEGF levels is yet to be established, studies have revealed a connection between mitochondrial dysfunction and VEGF expression. [42] LCLAT1 has been independently shown to cause oxidative stress-mediated mitochondrial dysfunction. [42] Hence, it is likely that down-regulation of VEGF may have contributed to the reduced expression of LCLAT1 in the polyplex treated cells. RFC5 (Replication factor C 5) is generally associated with the proliferation cell nuclear antigen (PCNA) [43] and has also been implicated in DNA damage repair. [43] A recent study has identified RFC5 as a novel oncogene in lung cancer. [44] Direct connection between RFC5 levels and VEGF expression is yet to be obtained. Nevertheless, independent studies have shown that RFC5 is regulated by FOXM1 (Forkhead box M1) while FOXO3 serves

as an antagonist for FOXM1 and VEGF in lung cancer. [45] Based on this evidence, it may be inferred that RFC5 and VEGF expression levels are directly correlated with each other. Our results further confirm this correlation as better VEGF silencing by the polyplex results in superior suppression of RFC5. The role of UBAP2 (Ubiquitin associated protein 2) in cancers remain inconclusive as some reports have suggested a tumor suppressor role in hepatocellular cancers [46] while few other studies on pancreatic cancer and glioblastoma have reported an oncogenic role for this gene.[47]

The overall picture of pathways differentially modulated by the polyplex treatment in A549 cells when compared with the free si-RNA shows that the regulation of greater number of genes involved in cancer signaling (Figure 11). This indicates that the VEGF silencing through the PVI polyplex has positive influence in inhibiting the progression of lung cancer cells.

Gene expression analysis

In gene expression analysis using RT-PCR, it was found that the polyplex treated cells showed a significant reduction in the expression levels of VEGF when compared with the untreated cells. However, the free si-RNA treated cells did not show significant reduction in the VEGF expression levels (Figure 12). This difference in silencing efficiency may be attributed to the superior ability of the polyplex to internalize in to the cells and a higher fraction of the polyplex being able to escape the endosome.

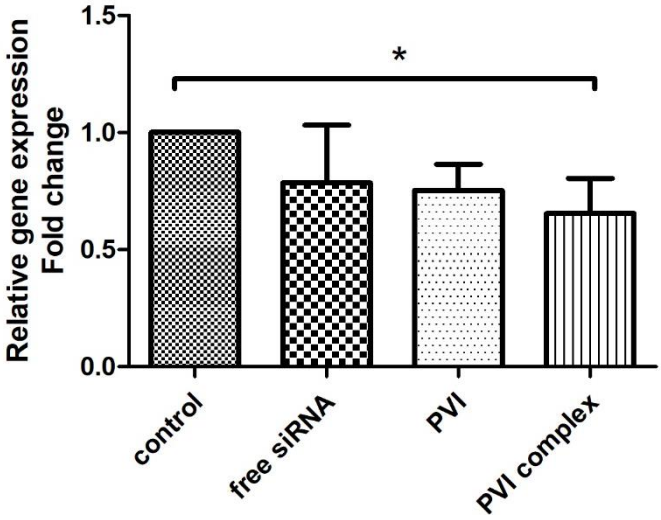

Figure12: Expression of Vascular endothelial growth factor (VEGF) mRNA in A549 cells analysed by reverse transcriptase polymerase chain reaction (RT-PCR). The results are represented as mean ± SD and analysed using one-way ANOVA followed by post hoc test using Bonferroni comparison test (n=3, * p<0.05).

Western blot studies

Figure 13 shows the VEGF protein levels quantified through Western blot analysis from cells treated with free si-RNA, blank PVI and polyplex.

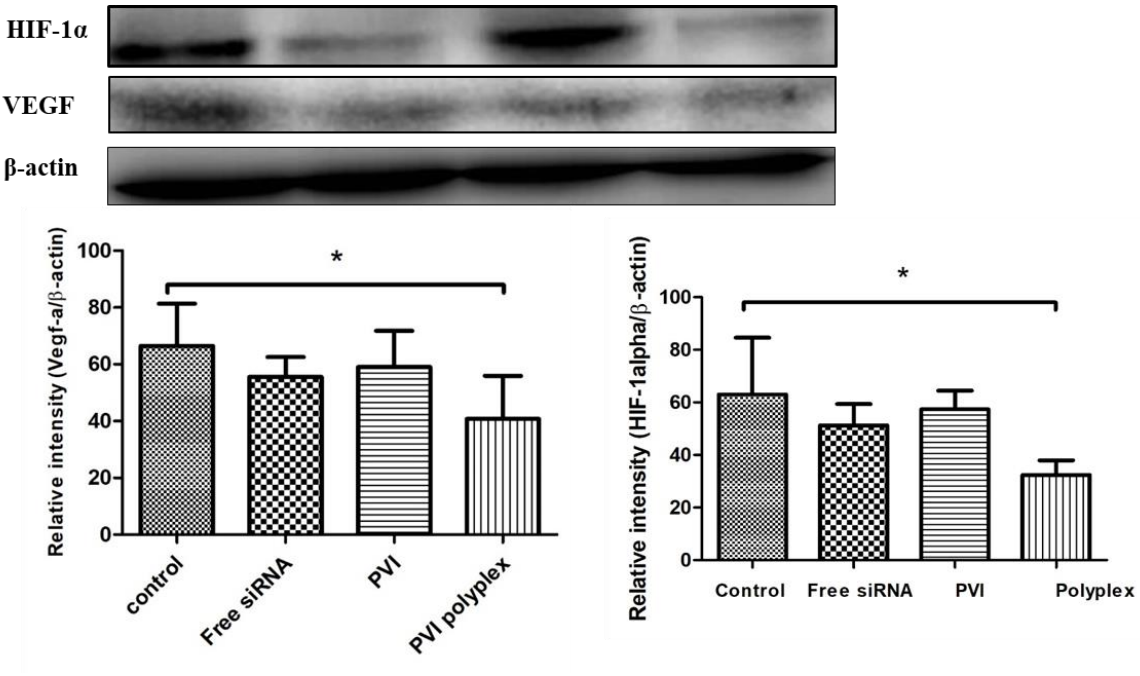

Figure 13: VEGF, HIF-1alpha and β-actin protein expression levels in A549 cells obtained from Western blot. The expression of VEGF and HIF-1 alpha was normalized to the corresponding β-actin. Data shown as mean ± SD of triplicate independent experiments *p<0.05 when compared to control.

A significant decrease in the VEGF levels was observed in cells treated with the polyplex when compared with the control cells suggesting that the polyplex mediates better internalization of the si-RNA. This is also reflected in the differential modulation of gene targets associated with VEGF in the microarray analysis. The superior silencing of VEGF by the polyplex is also reflected in the reduced levels of HIF-1α. Hypoxia inducible factor-1 alpha (HIF-1α) is expressed in oxygen deficient conditions and has been found to induce the expression of VEGF thereby promoting angiogenesis. [48] Recently, it has been found that HIF-1α and VEGF levels regulate each other through a competing endogenous RNA pathway involving mi-RNA. [49] Our data correlates with this finding as we find that silencing VEGF is reflected in a decrease in the HIF-1α levels also.

Concluding remarks

This work has demonstrated the capability of poly (1-vinyl imidazole) to serve as an efficient carrier of si-RNA for gene silencing. The effectiveness of this carrier is due to its better cellular internalization as well as its ability to escape the endosome. The silencing of VEGF resulted in altered expression levels of genes responsible for proliferation and metastasis of lung cancer cells as evidenced from the microarray analysis. In addition, VEGF silencing also resulted in enhanced cytotoxicity of the chemotherapeutic agent 5-flurouracil suggesting the promise of this strategy to be employed as an adjuvant therapy against lung cancer. Absence of cytotoxicity of the blank PVI polymer suggests that this carrier could be a cyto-compatible system for gene therapy.

Acknowledgement

The authors acknowledge financial support from a joint grant of the Department of Science Technology, India (INT/RUS/RSF/10) and Russian Science Foundation (6-45-02001). The infrastructural support from SASTRA Deemed University is also acknowledged.

References

(1) Zhao, Y.; Wang, W.; Guo, S.; Wang, Y.; Miao, L.; Xiong, Y.; Huang, L. PolyMetformin Combines Carrier and Anticancer Activities for in Vivo SiRNA Delivery. *Nat. Commun.* **2016**, *7* (May), 1–9. https://doi.org/10.1038/ncomms11822.

(2) Conte, C.; Mastrotto, F.; Taresco, V.; Tchoryk, A. Enhanced Uptake in 2D- and 3D- Lung Cancer Cell Models of Redox Responsive PEGylated Nanoparticles with Sensitivity to Reducing Extra- and Intracellular Environments. *J. Control. Release* **2018**, *277* (December 2017), 126–141.

(3) Nouri, N.; Talebi, M.; Palizban Abas, A. Viral and Nonviral Delivery Systems for Gene Delivery. *Advanced Biomedical Research*. 2012. https://doi.org/10.4103/2277-9175.98152.

(4) Peng, J.; Wu, Z.; Qi, X.; Chen, Y.; Li, X. Molecules 18, . *2013 SRC*, 7912–7929.

(5) Ihm, J. E.; Han, K. O.; Han, I. K.; Ahn, K. D.; Han, D. K.; Cho, C. S. High Transfection Efficiency of Poly(4-Vinylimidazole) as a New Gene Carrier. *Bioconjug. Chem.* **2003**, *14* (4), 707–708. https://doi.org/10.1021/bc025611q.

(6) Asayama, S.; Sekine, T.; Kawakami, H.; Nagaoka, S. Design of Aminated Poly(1-Vinylimidazole) for a New PH-Sensitive Polycation to Enhance Cell-Specific Gene Delivery. *Bioconjug. Chem.* **2007**, *18* (5), 1662–1667. https://doi.org/10.1021/bc700205t.

(7) Molina, M. J.; Gómez-AntóN, M. R.; Piérola, I. F. Factors Driving the Protonation of Poly(N-Vinylimidazole) Hydrogels. *J. Polym. Sci. Part B Polym. Phys.* **2004**, *42* (12), 2294–2307. https://doi.org/10.1002/polb.20104.

(8) Singha, K.; Namgung, R.; Kim, W. J. Polymers in Small-Interfering RNA Delivery. *Nucleic Acid Ther. (Formerly Oligonucleotides)* **2011**, *21* (3), 133–147.

https://doi.org/10.1089/nat.2011.0293.

(9) Pack, D. W.; Putnam, D.; Langer, R. Design of Imidazole-Containing Endosomolytic Biopolymers for Gene Delivery. *Biotechnol. Bioeng.* **2000**, *67* (2), 217–223. https://doi.org/10.1002/(SICI)1097-0290(20000120)67:2<217::AID-BIT11>3.0.CO;2-Q.

(10) Boztepe, C.; Tosun, E.; Bilenler, T.; Sislioglu, K. Synthesis and Characterization of Acrylamide-Based Copolymeric Hydrogel–Silver Composites: Antimicrobial Activities and Inhibition Kinetics against E. Coli. *Int. J. Polym. Mater. Polym. Biomater.* **2017**, *66* (18), 934–942. https://doi.org/10.1080/00914037.2017.1291513.

(11) Jeon, W.; Choi, Y.; Kim, H. Ultrasonics - Sonochemistry Ultrasonic Synthesis and Characterization of Poly (Acrylamide) - Co -Poly (Vinylimidazole)@ MWCNTs Composite for Use as an Electrochemical Material. *Ultrason. - Sonochemistry* **2018**, *43* (November 2017), 73–79. https://doi.org/10.1016/j.ultsonch.2017.11.024.

(12) Elella, M. H. A.; Mohamed, R. R.; ElHafeez, E. A.; Sabaa, M. W. Synthesis of Novel Biodegradable Antibacterial Grafted Xanthan Gum. *Carbohydr. Polym.* **2017**, *173*, 305–311. https://doi.org/10.1016/j.carbpol.2017.05.058.

(13) Hargrove, A. E.; Martinez, T. F.; Hare, A. A.; Kurmis, A. A.; Phillips, J. W.; Sud, S.; Pienta, K. J.; Dervan, P. B. Tumor Repression of VCaP Xenografts by a Pyrrole-Imidazole Polyamide. *PLoS One* **2015**, *10* (11), 9–13. https://doi.org/10.1371/journal.pone.0143161.

(14) Shi, B.; Zhang, H.; Shen, Z.; Bi, J.; Dai, S. Developing a Chitosan Supported Imidazole Schiff-Base for High-Efficiency Gene Delivery. *Polym. Chem.* **2013**, *4* (3), 840–850. https://doi.org/10.1039/c2py20494k.

(15) Gary, D. J.; Lee, H.; Sharma, R.; Lee, J. S.; Kim, Y.; Cui, Z. Y.; Jia, D.; Bowman, V. D.; Chipman, P. R.; Wan, L.; et al. Influence of Nano-Carrier Architecture on in Vitro SiRNA Delivery Performance and in Vivo Biodistribution: Polyplexes vs Micelleplexes. *ACS Nano* **2011**, *5* (5), 3493–3505. https://doi.org/10.1021/nn102540y.

(16) Hakamatani, T.; Asayama, S.; Kawakami, H. Synthesis of Alkylated Poly(1-Vinylimidazole) for a New PH-Sensitive DNA Carrier. *Nucleic Acids Symp. Ser.* **2008**, *52* (1), 677–678. https://doi.org/10.1093/nass/nrn342.

(17) Asayama, S.; Nishinohara, S.; Kawakami, H. Zinc-Chelated Poly(1-Vinylimidazole) and a Carbohydrate Ligand Polycation Form DNA Ternary Complexes for Gene Delivery. *Bioconjug. Chem.* **2011**, *22* (9), 1864–1868. https://doi.org/10.1021/bc2003378.

(18) Hassan, H. A. F. M.; Smyth, L.; Wang, J. T. W.; Costa, P. M.; Ratnasothy, K.; Diebold, S. S.; Lombardi, G.; Al-Jamal, K. T. Dual Stimulation of Antigen Presenting Cells Using Carbon Nanotube-Based Vaccine Delivery System for Cancer Immunotherapy. *Biomaterials* **2016**, *104*, 310–322. https://doi.org/10.1016/j.biomaterials.2016.07.005.

(19) Danilovtseva, E. N.; Zelinskiy, S. N.; Pal, V. A.; Kandasamy, G. Poly (1-Vinylimidazole) Prospects in Gene Delivery. *chinese J. Polym. Sci.* **2019**.

(20) Erdem, B. Synthesis and Characterization Studies of a Series of N-Vinyl Imidazole-Based Hydrogel. *ANADOLU Univ. J. Sci. Technol. A - Appl. Sci. Eng.* **2016**, *17* (5), 974–974. https://doi.org/10.18038/aubtda.265939.

(21) Vader, P.; Van Der Aa, L. J.; Engbersen, J. F. J.; Storm, G.; Schiffelers, R. M. Physicochemical and Biological Evaluation of SiRNA Polyplexes Based on PEGylated Poly(Amido Amine)S. *Pharm. Res.* **2012**, *29* (2), 352–361. https://doi.org/10.1007/s11095-011-0545-z.

(22) Nicolì, E.; Syga, M. I.; Bosetti, M.; Shastri, V. P. Enhanced Gene Silencing through Human Serum Albumin-Mediated Delivery of Polyethylenimine-SiRNA Polyplexes. *PLoS One* **2015**, *10* (4), 1–16. https://doi.org/10.1371/journal.pone.0122581.

(23) Johannes, L.; Lucchino, M. Current Challenges in Delivery and Cytosolic Translocation of Therapeutic RNAs. *Nucleic Acid Ther.* **2018**, *28* (3), 178–193. https://doi.org/10.1089/nat.2017.0716.

(24) Midoux, P.; Pichon, C.; Yaouanc, J. J.; Jaffrès, P. A. Chemical Vectors for Gene Delivery: A Current Review on Polymers, Peptides and Lipids Containing Histidine or Imidazole as Nucleic Acids Carriers. *Br. J. Pharmacol.* **2009**, *157* (2), 166–178. https://doi.org/10.1111/j.1476-5381.2009.00288.x.

(25) Sadremomtaz, A.; Mansouri, K.; Alemzadeh, G.; Safa, M.; Rastaghi, A. E.; Asghari, S. M. Dual Blockade of VEGFR1 and VEGFR2 by a Novel Peptide Abrogates VEGF-Driven Angiogenesis, Tumor Growth, and Metastasis through PI3K/AKT and MAPK/ERK1/2 Pathway. *Biochim. Biophys. Acta - Gen. Subj.* **2018**, *1862* (12), 2688–2700. https://doi.org/10.1016/j.bbagen.2018.08.013.

(26) Yang, W. J.; Yang, Y. N.; Cao, J.; Man, Z. H.; Li, Y.; Xing, Y. Q. Paxillin Regulates Vascular Endothelial Growth Factor A-Induced in Vitro Angiogenesis of Human Umbilical Vein Endothelial Cells. *Mol. Med. Rep.* **2015**, *11* (3), 1784–1792. https://doi.org/10.3892/mmr.2014.2961.

(27) Gupta, K.; Puri, A.; Shapiro, B. A. Functionalized Non-Viral Cationic Vectors for Effective SiRNA Induced Cancer Therapy. *DNA RNA Nanotechnol.* **2017**, *4* (1), 1–20. https://doi.org/10.1515/rnan-2017-0001.

(28) Sun, Q.; Wang, X.; Cui, C.; Li, J.; Wang, Y. Doxorubicin and Anti-VEGF SiRNA Co-Delivery via Nano-Graphene Oxide for Enhanced Cancer Therapy in Vitro and in Vivo. *Int. J. Nanomedicine* **2018**, *13*, 3713–3728. https://doi.org/10.2147/IJN.S162939.

(29) Zhao, X. G. J.-L. Focal Adhesion Kinase and Its Signaling Pathways in Cell Migration and Angiogenesis. *Adv. Drug Deliv. Rev.* **2012**, *63* (8), 610–615. https://doi.org/10.1016/j.addr.2010.11.001.Focal.

(30) Yang, Y.; Lu, Y.; Abbaraju, P. L.; Zhang, J.; Zhang, M.; Xiang, G.; Yu, C. Multi-Shelled Dendritic Mesoporous Organosilica Hollow Spheres: Roles of Composition and Architecture in Cancer Immunotherapy. *Angew. Chemie - Int. Ed.* **2017**, *56* (29), 8446–8450. https://doi.org/10.1002/anie.201701550.

(31) Yamaguchi, J.; Yokoyama, Y.; Kokuryo, T.; Ebata, T.; Enomoto, A.; Nagino, M. Trefoil Factor 1 Inhibits Epithelial-Mesenchymal Transition of Pancreatic Intraepithelial Neoplasm. *J. Clin. Invest.* **2018**, *128* (8), 3619–3629. https://doi.org/10.1172/JCI97755.

(32) Moss, S. F.; Lee, J.; Sabo, E.; Rubin, A. K.; Rommel, J.; Westley, R.; May, F. E. B.; Gao, J.; Meitner, P. A.; Tavares, R.; et al. NIH Public Access. *Cancer* **2009**, *14* (13), 4161–4167. https://doi.org/10.1158/1078-0432.CCR-07-4381.Decreased.

(33) Yu, Q.; Yin, L.; Jian, Y.; Li, P.; Zeng, W.; Zhou, J. Downregulation of PHF6 Inhibits Cell Proliferation and Migration in Hepatocellular Carcinoma. *Cancer Biother. Radiopharm.* **2019**, *34* (4), 245–251. https://doi.org/10.1089/cbr.2018.2671.

(34) Neuzillet, C.; Tijeras-Raballand, A.; Cohen, R.; Cros, J.; Faivre, S.; Raymond, E.; De Gramont, A. Targeting the TGFβ Pathway for Cancer Therapy. *Pharmacol. Ther.* **2015**, *147*, 22–31. https://doi.org/10.1016/j.pharmthera.2014.11.001.

(35) Costanza, B.; Rademaker, G.; Tiamiou, A.; De Tullio, P.; Leenders, J.; Blomme, A.; Bellier, J.; Bianchi, E.; Turtoi, A.; Delvenne, P.; et al. Transforming Growth Factor Beta-Induced, an Extracellular Matrix Interacting Protein, Enhances Glycolysis and Promotes Pancreatic Cancer Cell Migration. *Int. J. Cancer* **2019**. https://doi.org/10.1002/ijc.32247.

(36) Kim, W.; Kim, E. G.; Lee, S.; Kim, D.; Chun, J.; Park, K. H.; Youn, H. S.; Youn, B. H. TFAP2C-Mediated Upregulation of TGFBR1 Promotes Lung Tumorigenesis and Epithelial-Mesenchymal Transition. *Exp. Mol. Med.* **2016**, *48* (11), e273. https://doi.org/10.1038/emm.2016.125.

(37) Wang, J.; Zhao, W.; Guo, H.; Fang, Y.; Stockman, S. E.; Bai, S.; Ng, P. K. S.; Li, Y.; Yu, Q.; Lu, Y.; et al. AKT Isoform-Specific Expression and Activation across Cancer Lineages. *BMC Cancer* **2018**, *18* (1), 1–10. https://doi.org/10.1186/s12885-018-4654-5.

(38) Xie, Y.; Qi, Y.; Zhang, Y.; Chen, J.; Wu, T.; Gu, Y. Regulation of Angiogenic Factors by the PI3K/Akt Pathway in A549 Lung Cancer Cells under Hypoxic Conditions. *Oncol. Lett.* **2017**, *13* (5), 2909–2914. https://doi.org/10.3892/ol.2017.5811.

(39) Yin, M.; Tissari, M.; Tamminen, J.; Ylivinkka, I.; Rönty, M.; von Nandelstadh, P.; Lehti, K.; Hyytiäinen, M.; Myllärniemi, M.; Koli, K. Gremlin-1 Is a Key Regulator of the Invasive Cell Phenotype in Mesothelioma. *Oncotarget* **2017**, *8* (58), 98280–98297. https://doi.org/10.18632/oncotarget.21550.

(40) Rasheed, S. A. K.; Leong, H. S.; Lakshmanan, M.; Raju, A.; Dadlani, D.; Chong, F. T.; Shannon, N. B.; Rajarethinam, R.; Skanthakumar, T.; Tan, E. Y.; et al. GNA13 Expression Promotes Drug Resistance and Tumor-Initiating Phenotypes in Squamous Cell Cancers. *Oncogene* **2018**, *37* (10), 1340–1353. https://doi.org/10.1038/s41388-017-0038-6.

(41) Xiong, J. W.; Yu, Q.; Zhang, J.; Mably, J. D. An Acyltransferase Controls the Generation of Hematopoietic and Endothelial Lineages in Zebrafish. *Circ. Res.* **2008**, *102* (9), 1057–1064. https://doi.org/10.1161/CIRCRESAHA.107.163907.

(42) Guo, D.; Wang, Q.; Li, C.; Wang, Y.; Chen, X. VEGF Stimulated the Mitochondrial Functions Angiogenesis by Promoting The. *Oncotarget* **2017**, *8* (44), 77020–77027.

(43) Tomida, J.; Masuda, Y.; Hiroaki, H.; Ishikawa, T.; Song, I.; Tsurimoto, T.; Ohmori, H.; Todo, T. DNA Damage-Induced Ubiquitylation of RFC2 Subunit of Replication Factor C Complex * □. *J. Biol. Chem.* **2008**, *283* (14), 9071–9079. https://doi.org/10.1074/jbc.M709835200.

(44) Wang, M.; Xie, T.; Wu, Y.; Yin, Q.; Xie, S.; Yao, Q.; Xiong, J. I. E.; Zhang, Q. Identification of RFC5 as a Novel Potential Prognostic Biomarker in Lung Cancer through Bioinformatics Analysis. *Oncol. Lett.* **2018**, 4201–4210. https://doi.org/10.3892/ol.2018.9221.

(45) Karadedou, C. T.; Gomes, A. R.; Chen, J.; Petkovic, M.; Ho, K.; Zwolinska, A. K.; Feltes, A.; Wong, S. Y.; Chan, K. Y. K.; Cheung, Y.; et al. FOXO3a Represses VEGF Expression through FOXM1-Dependent and -Independent Mechanisms in Breast Cancer. *Oncogene* **2012**, No. June 2011, 1845–1858. https://doi.org/10.1038/onc.2011.368.

(46) Bai, D.; Wu, C.; Yang, L.; Zhang, C.; Zhang, P. UBAP2 Negatively Regulates the Invasion of Hepatocellular Carcinoma Cell by Ubiquitinating and Degradating Annexin A2. *Oncotarget* **2016**, *7* (22).

(47) Xu, H.; Zhang, Y.; Qi, L.; Ding, L.; Jiang, H.; Yu, H. NFIX Circular RNA Promotes Glioma Progression by Regulating MiR-34a-5p via Notch Signaling Pathway. *Front. Mol. Neurosci.* **2018**, *11* (July), 1–13. https://doi.org/10.3389/fnmol.2018.00225.

(48) Zimna, A.; Kurpisz, M. Hypoxia-Inducible Factor-1 in Physiological and Pathophysiological Angiogenesis: Applications and Therapies. *Biomed Res. Int.* **2015**, *2015*. https://doi.org/10.1155/2015/549412.

(49) Juan. HIF1A and VEGF Regulate Each Other by Competing Endogenous RNAmechanism and Involve in the Pathogenesis of Peritonealfibrosis. *Br. J. Psychiatry* **2018**, *111* (479), 1009–1010. https://doi.org/10.1192/bjp.111.479.1009-a.